Research Square

Preprints are preliminary reports that have not undergone peer review.
They should not be considered conclusive, used to inform clinical practice,
or referenced by the media as validated information.

Residential greenness and tuberculosis incidence across 1-km grids in Beijing: non-linear exposure-response and counterfactual health impact assessment

Ze Zeng
Army Medical University
Wenyi Zhang
Chinese PLA Center for Disease Control and Prevention
Zanmei Wei
Beijing Normal University
Zhidong Gao
Beijing Center for Disease Prevention and Control
Yuxiao Wang
Peking University
Junyu He
Zhejiang University
Hengliang Lv
Army Medical University
Yuming Guo
Monash University
Xingshu Chen
Army Medical University
Jie Li
Beijing Center for Disease Prevention and Control
Shanhua Sun
sunshanhua2010@126.com

Beijing Center for Disease Prevention and Control

Research Article

Keywords: Tuberculosis, Green space, Non-linear exposure–response, Health impact assessment, Spatial epidemiology, Beijing

Posted Date: November 12th, 2026

DOI: https://doi.org/10.21203/rs.3.rs-11426542/v1

License: This work is licensed under a Creative Commons Attribution 4.0 International License.
Read Full License

Additional Declarations: No competing interests reported.

Residential greenness and tuberculosis incidence across 1-km grids in Beijing: non-linear exposure-response and counterfactual health impact assessment

Ze Zeng[a,1], Wenyi Zhang[b,1], Zanmei Wei[c,1], Zhidong Gao[d], Yuxiao Wang[e,f],Junyu He[g], Hengliang Lv[a], Yuming Guo[h], Xingshu Chen[a,*] ,Jie Li [d,i,*], Shanhua Sun[d,i,*]

[a] Department of Military Medical Geography, Army Medical Training Base, Army Military Medical University, Chongqing, China.

[b] Chinese PLA Center for Disease Control and Prevention, Beijing, China.

[c] Faculty of Geographical Science, Beijing Normal University, Beijing, China.

[d] Beijing Institute of Tuberculosis Control, Beijing Center for Disease Prevention and Control, Beijing, China.

[e] National Institute of Health Data Science, Peking University, Beijing, China.

[f] Institute of Medical Technology, Peking University Health Science Center, Beijing, China.

[g] Ocean Academy, Ocean College, Zhejiang University, Zhoushan, China.

[h] Department of Epidemiology and Preventive Medicine, School of Public Health and Preventive Medicine, Monash University, Melbourne, VIC, Australia.

[i] Capital Medical University, Beijing, China.

[1]The co-first authors.

[*]Corresponding authors: xingshuchen2011@163.com, lijie304304@163.com, sunshanhua2010@126.com.

Abstract

In hyper-dense megacities, rapid urbanization and constrained access to nature may compound the risk of airborne infectious diseases such as tuberculosis (TB), yet fine-scale epidemiological evidence linking green space to TB incidence remains limited. We conducted a 13-year population-based panel study tracking 5,712 populated 1-km grid cells across Beijing, China (2012–2024). Using a Poisson two-way fixed-effects framework adjusting for district and temporal fixed effects, time-varying meteorology, and co-pollutants, long-term vegetation exposure (12-month moving average NDVI) showed a robust protective association, with a 43.3% risk reduction per one-IQR increase (IRR = 0.567, 95% CI: 0.557–0.578). Rather than a conventional log-linear response, we identified a pronounced non-linear, L-shaped exposure–response curve — corroborated by non-parametric decile binning —with the steepest risk reductions occurring in vegetation-deprived built environments before plateauing at higher greenness levels, consistent with biological saturation. Translating this function into three counterfactual greening scenarios showed that while universal greening (+0.1 NDVI city-wide) maximized absolute burden reduction, targeting dual-vulnerable grids—simultaneously high in population density and low in greenness—achieved an intervention efficiency nearly four times greater, averting over a quarter of city-wide cases (27.33%) by intervening in only 15.7% of spatial cells. These findings indicate that the health dividend of urban greening is governed as much by spatial allocation as by total quantity, providing an evidence base for integrating precision environmental health governance into municipal spatial planning.

Keywords: Tuberculosis; Green space; Non-linear exposure–response ;Health impact assessment; Spatial epidemiology; Beijing

1.Introduction

Tuberculosis (TB), caused by *Mycobacterium tuberculosis*, remains one of the leading infectious causes of mortality worldwide, posing an enduring challenge to global public health(Zenner et al., 2026). Despite substantial progress driven by the World Health Organization's (WHO) End TB Strategy, achieving its ambitious reduction targets remains constrained by multi-drug resistance, diagnostic and therapeutic

delays, and persistent socioeconomic inequalities(Hui et al., 2026; Lönnroth et al., 2010) . Rapid global urbanization has further concentrated massive populations into hyper-dense metropolitan environments, where overcrowding, compromised indoor ventilation, and prolonged psychological distress create conditions conducive to sustained aerosol transmission and reactivation of latent TB infection (LTBI)(Furin et al., 2019; Prasad et al., 2016) . While conventional control paradigms rely primarily on biomedical therapeutics and post-onset case detection, these downstream clinical approaches exhibit diminishing marginal returns against widespread community reservoirs(Furin et al., 2019; Zenner et al., 2026). Identifying upstream, modifiable environmental determinants that reinforce host biological resistance and curtail transmission pathways has therefore emerged as an important frontier for resilient, health-centered urban governance(Hui et al., 2026; Twohig-Bennett and Jones, 2018).

Ambient green space, a core component of nature-based urban health solutions, confers broad benefits including reduced all-cause mortality, mitigated cardiovascular risk, and enhanced respiratory function(Cao et al., 2025; Rojas-Rueda et al., 2019). Biologically, natural vegetation may reinforce host cell-mediated defense — the physiological cornerstone of granuloma integrity and latent TB containment — through several converging pathways(Ge et al., 2021; Martin et al., 2025). Contact with residential greenery is associated with attenuated hypothalamic-pituitary-adrenal (HPA) axis activity and reduced cortisol-mediated immunosuppression(Jones et al., 2021), while promoting outdoor sun exposure that stimulates vitamin D synthesis and upregulates antimicrobial peptide (cathelicidin) expression in alveolar macrophages(Liu et al., 2006; Yamshchikov et al., 2010). Vegetative canopies may additionally act as physical filters that reduce exposure to ambient air pollutants, preserving respiratory mucosal clearance(Martin et al., 2025; Wang et al., 2022).

However, translating these biological mechanisms into population-level epidemiological evidence has been constrained by methodological limitations. Existing investigations into residential greenness and TB have predominantly relied on coarse administrative aggregations (e.g., district- or county-level metrics) or treated vegetation as a secondary covariate within air pollution time-series models rather than as a primary exposure of interest(Yuan et al., 2025; Zhu et al., 2022). Such coarse spatial aggregation risks ecological fallacy and exposure misclassification by smoothing out contrasts between densely built quarters and adjacent green belts(Wang et al., 2025). Moreover, individual-level cohort studies of greenness and TB have focused almost exclusively on mortality or drug-resistant subsets(Song et al., 2024; Wang et al., 2022) , leaving high-resolution, population-based incidence dynamics

comparatively unexplored.

Prior environmental studies have predominantly assumed a log-linear relationship between greenness exposure and health outcomes(Rojas-Rueda et al., 2019; Twohig-Bennett and Jones, 2018), a specification that may obscure non-linear biological thresholds and diminishing marginal returns. We hypothesize that incremental greenery confers disproportionately larger protective benefit in severely vegetation-deprived built environments — a pattern we conceptualize as "deficit relief" — whereas in already-green environments, outdoor vegetation gains may be insufficient to offset crowded indoor transmission dynamics, potentially yielding a saturating plateau(Prasad et al., 2016). Furthermore, empirical evaluations have rarely moved beyond static relative risk estimates to simulate prospective, counterfactual greening scenarios(Martin et al., 2025; Rojas-Rueda et al., 2019). Consequently, urban planning authorities in land-constrained megacities lack an evidence base for deciding whether limited municipal greening budgets should pursue universal city-wide expansion or geographically targeted interventions in ecologically and demographically vulnerable areas(Barboza et al., 2021; Martin et al., 2025).

To address these evidence gaps, we conducted a 13-year population-based panel study across Beijing, China (2012–2024), tracking 5,712 populated 1-km × 1-km grid cells. Using a high-resolution Poisson two-way fixed-effects framework adjusting for district-level spatial heterogeneity, secular and seasonal trends, time-varying meteorology, and collinearity-screened co-pollutants, we aimed to: (1) evaluate the independent, long-term association between residential greenness and active pulmonary tuberculosis incidence at a fine spatial scale; (2) characterize the functional form of this exposure–response relationship using natural cubic splines and non-parametric decile binning to test for non-linearity and saturation; and (3) translate these estimates into counterfactual health impact assessments across three policy scenarios, quantifying spatial efficiency trade-offs to inform precision urban greening strategies.

2. Materials and Methods

2.1 Tuberculosis Case Data

This study utilized individual-level active tuberculosis notification records in Beijing, provided by the Beijing Municipal Center for Disease Control and Prevention. The registry encompasses a 14-year surveillance period spanning January 2011 through December 2024. Each reported case was characterized by confirmed onset date and

residential address; all identifying information was fully anonymized prior to data transfer. Cases were geocoded based on residential location and spatially assigned to a 1 km × 1 km fishnet grid system covering the entire administrative territory of Beijing, which was partitioned into 16,735 grid cells in total. Monthly case counts were subsequently tabulated for each grid cell to construct the spatiotemporal panel dataset used in downstream analyses.

2.2 Environmental and Socioeconomic Variables

Monthly meteorological variables—including mean temperature, relative humidity, precipitation, and wind speed—were derived from the CDMet 4 km daily gridded meteorological reanalysis product for mainland China(Zhang et al., 2024). Monthly NDVI, serving as the primary indicator of urban green space, was obtained from the MODIS/Terra Vegetation Indices Monthly Level-3 Global 1 km SIN Grid V061 product(Didan, 2021). Nighttime light intensity, used as a proxy for socioeconomic development, was extracted from the global annual 500 m resolution NPP-VIIRS-like nighttime light dataset(Chen et al., 2021). Ambient population distribution was sourced from the LandScan Global dataset, which provides annual population estimates at 1 km spatial resolution(Sims et al., n.d.) . Ground-level concentrations of O_3 and $PM_{2.5}$ were obtained from the ChinaHigh seamless 1 km daily datasets, respectively(Wei et al., 2020; Yang et al., 2025). Concentrations of NO_2, SO_2, and CO were acquired from the ChinaHighAirPollutants (CHAP) database, which delivers daily seamless 1 km surface-level estimates across China (Wei et al., 2023).

All variables were harmonized to a common 1 km × 1 km monthly panel format. For spatial harmonization, variables available at resolutions finer than 1 km were aggregated to the target grid via area-weighted averaging, whereas variables at coarser resolutions were resampled using centroid-based extraction. For temporal harmonization, daily observations were averaged to calendar-month means, and sub-monthly composite products were collapsed within each month accordingly. The complete dataset covers January 2011 to December 2024; however, the analytical sample is restricted to January 2012 onwards, as the 12-month backward moving average of NDVI requires one full year of antecedent observations (see Section 2.3).

2.3 Statistical Model, Co-pollutant Selection, and Sensitivity Analyses

To estimate the association between green space exposure and tuberculosis (TB) incidence at high spatial resolution, we employed a Poisson two-way fixed-effects regression model. The unit of analysis was the 1-km × 1-km grid cell per month. Grid cells with a mean monthly resident population fewer than 500 were excluded from

model fitting to minimize statistical artifacts arising from structural zero inflation and sparse count data. The logarithm of monthly resident population in each grid cell was incorporated as an offset term to represent the baseline population at risk. Concurrently, log-transformed population density was included as a time-varying covariate to capture the independent epidemiological influence of localized environmental crowding and social contact pressure, as well as to relax the rigid assumption of proportional population scaling inherent in standard offset formulations. The model is specified as follows:

$$\log(\mathrm{E}[Y_{it}]) = \log(POP_{it}) + \beta \cdot NDVI_{MA12,it} + \gamma \cdot \mathrm{X_{it}} + \alpha_{dis} + \delta_t$$

where $Y_{i,t}$ represents the TB case count in grid i during month t; β represents the log incidence rate ratio (IRR) associated with a one-IQR increase in the 12-month backward moving average NDVI ($NDVI_{MA12,it}$); X_{it} is a vector of time-varying covariates, including meteorological factors (mean temperature and its quadratic term, relative humidity and its quadratic term, precipitation, and wind speed), nighttime light intensity, and population density; spatial fixed effects (α_{dis}) were specified at the administrative district level to control for time-invariant district-level confounders, and temporal fixed effects (δ_t) were specified at the year-month level to account for seasonality and secular trends. To account for potential spatial dependency and serial autocorrelation among grid cells within the same administrative unit, cluster-robust standard errors were estimated by clustering at the district level.

The 12-month backward moving average NDVI ($NDVI_{MA12}$) was selected as the primary green space exposure, as the protective mechanisms of green space on tuberculosis are expected to operate through chronic cumulative pathways rather than acute short-term effects, and a 12-month window spanning a complete annual cycle minimizes exposure misclassification arising from Beijing's pronounced seasonal vegetation oscillation(Zhu et al., 2022).

Prior to model estimation, we systematically assessed collinearity among the six candidate co-pollutants ($PM_{2.5}$, SO_2, PM_{10}, O_3, NO_2, and CO, all as 6-month lagged means) using pairwise Pearson correlations and variance inflation factors (VIF). Strong intercorrelations were identified among $PM_{2.5}$, PM_{10}, NO_2, and CO (Pearson r = 0.84–0.97; Supplementary Figure S1), with VIF values exceeding acceptable thresholds for $PM_{2.5}$ (VIF = 44.96), PM_{10} (VIF = 26.26), and CO (VIF = 22.55; Supplementary Figure S2). To mitigate collinearity bias while retaining adequate pollution control, NO_2 (VIF = 10.83; representative of traffic and combustion emissions) and O_3 (VIF = 3.09; representative of photochemical pollution, r = −0.61

with NO_2) were retained as co-pollutant control variables in the primary model, and all exposure variables were standardized to their respective IQRs to facilitate interpretation.

To verify the robustness of the primary findings, three sensitivity analyses were conducted. First, we replaced the 12-month lagged NDVI moving average with a 6-month moving average ($NDVI_{MA6}$) to assess whether the exposure lag window influenced the estimated association. Second, the years 2020–2022 were excluded to evaluate whether COVID-19-related control measures, which substantially altered population mobility and healthcare-seeking behavior during this period, confounded the observed NDVI–TB relationship. Third, the primary model was re-estimated with all six air pollutants ($PM_{2.5}$, SO_2, PM_{10}, O_3, NO_2, and CO) included simultaneously as co-pollutants, to confirm that the parsimonious pollutant selection strategy did not materially affect the NDVI effect estimate.

2.4 Non-linear Exposure-Response Relationship and Binned Validation

To investigate the non-linear dose-response relationship between long-term green space exposure and TB incidence, we incorporated a natural cubic spline function (df = 3) for the 12-month moving average NDVI ($NDVI_{MA12}$) into the grid-level two-way fixed-effects Poisson framework. The degrees of freedom were set to 3, balancing model flexibility with parsimony given the expected monotonic protective shape of the NDVI – TB association. Relative risks (RRs) were calculated using the 10th percentile of the NDVI distribution (P_{10} = 0.279) as the centering reference point, representing the lowest greenery stratum in Beijing's urban landscape. The spline model was fully adjusted for all time-varying meteorological and socioeconomic covariates, alongside IQR-standardized co-pollutants (NO_2 and O_3, lag 6m).

To non-parametrically validate the shape of the spline-derived exposure-response curve, we additionally conducted a binned relative risk analysis. The NDVI distribution (restricted to the P1 – P99 range) was divided into 10 equal-frequency decile bins, and a separate Poisson fixed-effects model was fitted with each bin represented as a dummy variable. The bin whose mean NDVI was closest to P_{10} served as the reference category (RR = 1), consistent with the spline centering point. This non-parametric approach imposes no functional form assumption on the exposure-response relationship, providing an independent check on whether the spline-derived curve shape reflects the underlying data pattern.

2.5 Counterfactual Health Impact Assessment

To quantify the potential tuberculosis burden reduction achievable through green space improvement, we conducted a counterfactual health impact assessment under three policy scenarios. For each 1-km grid cell *i*, the long-term baseline NDVI exposure ($\overline{NDVI_i}$) was defined as the mean of all monthly NDVI ($NDVI_{MA12}$) observations from 2012 to 2024. The counterfactual NDVI ($NDVI_i^*$) was then specified according to each scenario. The scenario-specific incidence rate ratio for grid *i* was derived directly from the non-linear exposure-response curve:

$$RR_i^{scenario} = \exp\left[f(NDVI_i^*) - f\left(\overline{NDVI_i}\right)\right]$$

where *f()* denotes the natural cubic spline function estimated in Section 2.4. Because the counterfactual and baseline predictions are evaluated on the same spline and referenced against the same anchor point, the centering reference cancels out in the difference, rendering the result independent of the reference point choice. The Prevented Fraction for grid *i* was subsequently calculated as:

$$PF_i = 1 - RR_i^{scenario}$$

and the annual number of avoidable tuberculosis cases was estimated as:

$$\Delta Cases_i = \overline{Cases_i} \times PF_i$$

where $\overline{Cases_i}$ denotes the multi-year mean annual TB case count in grid *i*, computed by summing monthly counts within each calendar year and averaging across all study years. City-wide totals were obtained by aggregating grid-level estimates. To prevent unreliable extrapolation beyond the observed data range, baseline NDVI values below the 1st percentile were truncated to that lower bound, and counterfactual NDVI values exceeding the 99th percentile were capped accordingly. Uncertainty in the spline coefficients was propagated to PF_i using the joint delta method applied to the spline basis difference vector, yielding 95% confidence intervals.

Three counterfactual scenarios were evaluated. Scenario 1 (district-level gap-filling) raised grids with NDVI below the district-specific 25th percentile to the district-specific median, reflecting an equity-oriented policy targeting the most vegetation-deprived areas within each administrative unit. Scenario 2 (universal greening) applied a uniform increase of +0.1 NDVI units across all grids, simulating a city-wide greening initiative. Scenario 3 (targeted high-risk intervention) intervened only in grids simultaneously meeting high population density (at or above the city-wide 75th percentile) and low vegetation cover (below the city-wide 25th percentile), raising these dual-vulnerable grids to the city-wide median NDVI, representing an efficiency-oriented strategy prioritising areas where health need and

greenery deficit coincide. Only grid cells with a mean population ≥500 were included in all scenarios, consistent with the primary model.

To synthesize spatial patterns for policy interpretation, districts were grouped into three functional zones adapted from Beijing's official four-zone spatial planning framework: the Capital Function Core Zone (Dongcheng and Xicheng) was merged with the contiguous Urban Function Extended Zone (Chaoyang, Haidian, Fengtai, and Shijingshan) into a single "Urban Built-up Zone" owing to the core zone's compact spatial footprint (<1% of municipal land area), while the Urban Development Zone (Tongzhou, Shunyi, Daxing, Changping, and Fangshan) and the Ecological Conservation Zone (the remaining five outer districts: Mentougou, Pinggu, Huairou, Miyun, and Yanqing) were retained as defined.

3. Results

3.1 Descriptive Statistics and Spatiotemporal Patterns

Between 2012 and 2024, a total of 88,757 active tuberculosis (TB) cases were officially registered across Beijing (Table 1). Following the exclusion of sparsely populated cells (mean population < 500), the final analytical dataset comprised 891,072 grid-months across 5,712 grid cells (Table 1). Among grid-months with documented cases (67,692 observations, 7.6%), the monthly notification count averaged 1.31 cases (SD: 0.81; range: 1–50) per active cell (Table 1). The primary exposure, 12-month moving average NDVI ($NDVI_{MA12}$), had an overall mean of 0.373 (SD: 0.072; IQR: 0.322–0.424) (Table 1). Selected co-pollutants (NO_2 and O_3) alongside supporting meteorological and socioeconomic covariates exhibited substantial spatiotemporal heterogeneity (Table 1).

Temporal and spatial dynamics revealed distinct patterns between vegetation greenness and TB burden (Figure 1). Temporally, monthly TB notifications exhibited a steady secular decline coupled with seasonal fluctuations, whereas ambient NDVI followed a near-stationary decadal trend (+0.0070 units/year) dominated by recurrent seasonal cycles (Figure 1a, b). Spatially, a pronounced geographic mismatch was observed: while high vegetation greenness was predominantly concentrated in peripheral ecological conservation zones, active TB cases were heavily clustered within high-density central urban districts and peri-urban corridors (Figure 1c, d).

Table 1. Descriptive Statistics of Study Variables (Beijing, 2012–2024)

Variable	Unit	Mean (SD)	Median (IQR)	Range

Outcome				
Monthly TB cases[1]	count	1.31 (0.81)	1.00 (1.00–1.00)	1–50
88,757 total cases; **67,692** of 891,072 grid-months had ≥1 case (7.6%)				
Primary Exposure				
NDVI (12-month lagged mean)[2]	index	0.373 (0.072)	0.374 (0.322–0.424)	0.117–0.689
Co-pollutant Control Variables (6-month lagged mean, VIF-selected)				
Nitrogen dioxide (NO_2)	μg/m³	39.6 (13.1)	38.6 (29.2–49.1)	9.8–86.1
Ozone (O_3)	μg/m³	91.2 (26.8)	88.9 (66.9–115.4)	28.8–150.4
Meteorological Covariates (current-month values)				
Mean temperature	°C	13.0 (10.9)	14.0 (2.5–22.9)	−11.5–29.0
Relative humidity	%	54.8 (13.0)	54.2 (43.9–65.3)	28.1–86.6
Precipitation	mm	50.4 (75.7)	19.2 (3.6–67.7)	0.0–576.4
Wind speed	m/s	2.19 (0.49)	2.15 (1.80–2.56)	1.07–4.29
Socioeconomic Covariates (current-month values)				
Population density	persons/km²	3,411 (5,208)	1,416 (818–2,990)	6–44,377
Nighttime light intensity (NTL)	nW/cm²/sr	12.46 (13.92)	6.84 (2.62–18.45)	0.00–169.78
Excluded Co-pollutants (current-month values)				
$PM_{2.5}$	μg/m³	56.0 (28.4)	49.9 (35.2–70.2)	11.9–202.6
PM_{10}	μg/m³	95.4 (39.2)	88.3 (67.5–121.0)	22.5–273.5
SO_2	μg/m³	14.1 (14.7)	8.2 (5.8–15.7)	1.2–125.5
CO	mg/m³	1.00 (0.55)	0.83 (0.63–1.16)	0.19–3.73

Statistics computed from 891,072 grid-month observations (5,712 grids with mean population ≥500, selected from 16,735 total 1-km × 1-km grids covering Beijing; 2012–2024). IQR = interquartile range (P_{25}–P_{75}); SD = standard deviation; NDVI = Normalized Difference Vegetation Index; NTL = nighttime light intensity; VIF = variance inflation factor.

[1] Statistics computed among grid-months with at least one TB case (67,692 of 891,072 grid-months, 7.6%; pop≥500 grids only).

[2] 12-month backward moving average of monthly NDVI, used as the primary exposure variable in all models.

Excluded co-pollutants: $PM_{2.5}$, PM_{10}, SO_2, and CO were excluded from the primary model following VIF-based collinearity screening. Concurrent monthly values shown for reference; 6-month lagged means were used in the sensitivity analysis (SA3).

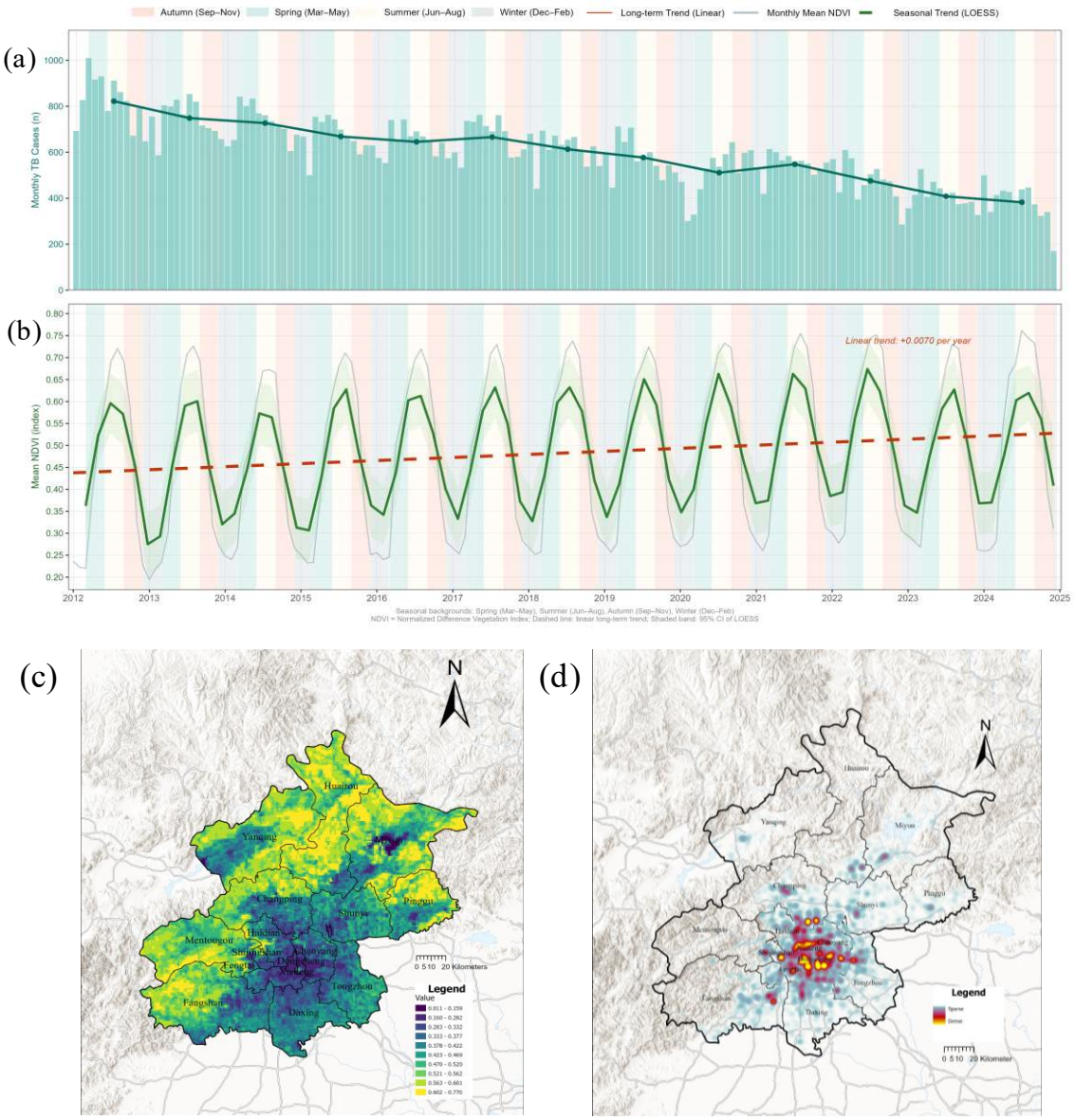


Figure 1. Temporal trends and spatial distributions of tuberculosis (TB) incidence and vegetation greenness (NDVI) across Beijing, 2012–2024.

(a) Monthly city-wide aggregated TB notification counts (teal bars) with overlaid annual mean secular trend (dark solid line with square markers) across four distinct seasons. **(b)** Monthly mean ambient NDVI (grey solid line) and LOESS smoothed seasonal oscillation (dark green line with light green 95% confidence bands), displaying a minimal linear decadal slope of +0.0070 units per year (red dashed line). **(c)** Spatial distribution of multi-year mean NDVI across 1-km × 1-km grid cells over Beijing's administrative districts. **(d)** Spatial kernel density heat map of cumulative active TB notifications, illustrating dense epidemiological disease clustering across the central urban core and peri-urban corridors.

3.2 Association Between Green Space and Tuberculosis Incidence and Sensitivity Analyses

In the fully adjusted two-way fixed-effects Poisson model, long-term residential greenness exposure was strongly and inversely associated with tuberculosis incidence

(Table 2). Each one-IQR increase in the 12-month moving average NDVI ($NDVI_{MA12}$, IQR= 0.102) corresponded to a 43.3% reduction in TB risk (IRR = 0.567, 95% CI: 0.557–0.578, $P < 0.001$). Conversely, 6-month lagged NO_2 (IRR = 1.618, 95% CI: 1.552–1.687) and O_3 (IRR = 1.394, 95% CI: 1.224–1.588) were positively associated with TB notifications (Table 2).

The protective association of green space remained highly robust across all sensitivity analyses (Supplementary Figure S3). Shortening the exposure lag window to a 6-month moving average ($NDVI_{MA6}$) yielded a consistent protective effect (IRR = 0.458, 95% CI: 0.446–0.471). Furthermore, effect estimates were virtually unchanged when excluding the COVID-19 pandemic period (2020–2022; IRR = 0.550, 95% CI: 0.539–0.561) or simultaneously controlling for all six candidate air pollutants (IRR = 0.561, 95% CI: 0.550–0.571).

Table 2. Association of Green Space (NDVI) and Air Pollutants with Tuberculosis Incidence in Beijing: Poisson Two-way Fixed-Effects Model (2012–2024)

Variable	IQR (unit)	IRR	95% CI	*P*-value	Sig.
Primary Exposure					
NDVI (lag 12m)	0.102 (index)	0.567	0.557–0.578	<0.001	***
Co-pollutant Control Variables					
NO_2 (lag 6m)	19.85 (μg/m³)	1.618	1.552–1.687	<0.001	***
O_3 (lag 6m)	48.47 (μg/m³)	1.394	1.224–1.588	<0.001	***
Meteorological Covariates (current-month values)					
Mean temperature (°C)	—	1.059	1.030–1.089	<0.001	***
Mean temperature² (°C²)	—	1.001	1.000–1.001	0.018	*
Relative humidity (%)	—	1.042	1.018–1.066	<0.001	***
Relative humidity² (%²)	—	1.000	1.000–1.000	0.027	*
Precipitation (mm)	—	1.001	1.000–1.001	0.048	*
Wind speed (m/s)	—	1.717	1.589–1.854	<0.001	***
Socioeconomic Covariates (current-month values)					
log(Population density)	—	0.590	0.584–0.596	<0.001	***
log(Nighttime light intensity)	—	1.536	1.513–1.559	<0.001	***

Fixed effects: District (n=16) + Year-month **Offset:** log(population) **Grids (pop≥500):** 5,712 **Observations:** 891,072 grid-months **Excluded co-pollutants:** $PM_{2.5}$, PM_{10} , CO , SO_2

IRR = incidence rate ratio; CI = confidence interval; IQR = interquartile range; NDVI = Normalized Difference Vegetation Index; VIF = variance inflation factor.

All exposure and co-pollutant variables were IQR-standardized; IRR represents the change in tuberculosis incidence

per one-IQR increase. NDVI: 12-month lagged mean. Air pollutants: 6-month lagged mean. Meteorological and socioeconomic covariates were not IQR-standardized ; IRR represents per-unit change.

Co-pollutant selection: $PM_{2.5}$, PM_{10}, and CO were excluded due to severe multicollinearity (VIF > 20). SO_2 was excluded due to its lower relevance to traffic/photochemical pathways and residual collinearity. NO_2 and O_3 were retained as representative indicators of traffic/combustion and photochemical pollution, respectively (see Supplementary Figures S1–S2).

Significance codes: *** $P<0.001$; ** $P<0.01$; * $P<0.05$. Data period: 2012–2024. Population filter: grid-level mean population ≥500 persons.

3.3 Non-linear Exposure–Response Relationship and Binned Validation

The fully adjusted natural cubic spline model revealed a pronounced non-linear, monotonic protective relationship between long-term NDVI exposure and tuberculosis incidence (Figure 2). Relative to the 10th percentile reference (P_{10} = 0.279), disease risk escalated sharply in vegetation-deprived areas (RR = 1.327, 95% CI: 1.299 – 1.356 at P_1). Across the lower-to-middle exposure spectrum, risk dropped rapidly to an RR of 0.544 (95% CI: 0.532 – 0.556) at the median (P_{50} = 0.374), beyond which the curve exhibited diminishing marginal protective returns, gradually leveling off toward the upper exposure bound (RR = 0.272, 95% CI: 0.246 – 0.300 at P_{99}).

The non-parametric binned decile analysis closely corroborated this non-linear trajectory (Supplementary Figure S4). Relative to the reference decile (D2, mean NDVI = 0.297), the lowest greenness decile (D1, mean NDVI = 0.258) exhibited a significantly heightened TB risk (RR = 1.192, 95% CI: 1.168–1.216, $P < 0.001$). Across higher exposure deciles, risk decreased monotonically, reaching RR = 0.653 (95% CI: 0.631–0.675) in D5 and RR = 0.341 (95% CI: 0.321–0.362) in D10. The close alignment between the categorical estimates and the continuous spline verified that the observed sub-linear protective pattern was not an artifact of spline parameterization.

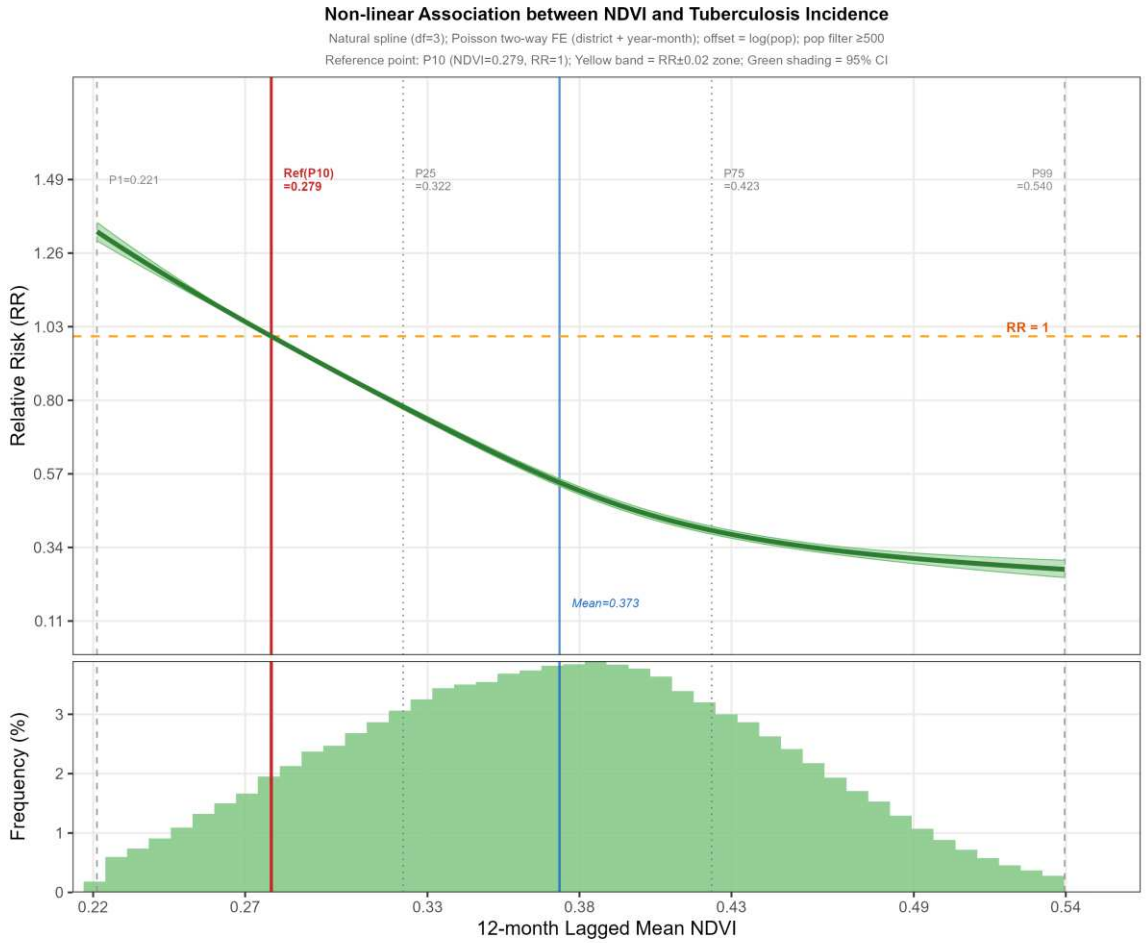


Figure 2. Non-linear exposure–response relationship between 12-month lagged NDVI and tuberculosis incidence in Beijing (2012–2024).

The upper panel displays the relative risk (RR, solid green line) with 95% confidence intervals (shaded green area) estimated via a natural cubic spline function (*df* = 3) in the Poisson two-way fixed-effects model, centered at the 10th percentile (P_{10} = 0.279, RR = 1.000, vertical red line). Vertical dotted grey lines denote key percentiles (P_1, P_{25}, P_{75}, and P_{99}), and the solid blue line indicates the mean exposure (NDVI = 0.373). The lower panel shows the exposure frequency distribution of 12-month lagged NDVI across study grid-months.

3.4 Counterfactual Health Impact Assessment and Scenario Comparison

Counterfactual simulations across the three policy scenarios demonstrated substantial reductions in tuberculosis incidence, accompanied by distinct spatial benefit configurations and planning zone dynamics (Table 3, Figure 3, and Figure 4). Under Scenario 1 (district-level gap-filling), an estimated 1,336.7 active TB cases (95% CI: 1,294.6–1,377.9) were avoidable annually city-wide, achieving an overall prevented fraction (PF) of 19.58% (95% CI: 18.96%–20.18%). Spatially, elevated grid-level PF values (>30%) were dispersed primarily across peripheral and suburban territories (Figure 3a), with the Urban Development Zone capturing the largest health dividend (670.8 cases/year, a 27.2% reduction from its baseline; led by Changping, Tongzhou, and Daxing), whereas central districts saw minimal gains owing to compressed

baseline greenness distributions and narrow within-district P_{25}–P_{50} increments (Figure 4a).

Under Scenario 2 (universal greening), city-wide reductions peaked at 3,067.2 avoidable cases annually (95% CI: 2,944.3–3,185.2; PF = 44.92%, 95% CI: 43.12%–46.65%). Spatially, elevated grid-level PF values (>40%–49%) formed a contiguous high-benefit expanse across the central core and dense urban built-up areas, reflecting steep marginal protection across vegetation-deprived grids compared to saturated, attenuated gains in peripheral ecological zones (Figure 3b). Driven by large resident populations, the Urban Built-up Zone captured over half of all city-wide avoidable cases (1,761.0 cases/year; led by Chaoyang, Haidian, and Fengtai), followed by the Urban Development Zone (1,089.6 cases/year) (Figure 4b).

Under Scenario 3 (targeted high-risk intervention), 1,865.8 TB cases were prevented per year (95% CI: 1,816.2–1,913.9; PF = 27.33%, 95% CI: 26.60%–28.03%), with health benefits overwhelmingly concentrated within the central Urban Built-up Zone (73.5% of total avoidable cases; Figure 3c and Figure 4c). This targeted strategy produced substantial local burden reductions in the historical core (averting 51.0% of cases in Xicheng and 40.7% in Dongcheng) as well as dense urban corridors across Chaoyang and Fengtai (Figure 4c).

Cross-scenario evaluation highlighted a fundamental trade-off between absolute intervention scale, geographical equity, and spatial resource efficiency (Table 3). Although universal greening (Scenario 2) attained the largest absolute reduction by intervening across all 5,712 eligible grids, its per-grid return was the lowest (0.54 avoidable cases/grid/year; efficiency ratio: 30.7; Table 3) due to diminishing marginal protection in already-green outer areas. District gap-filling (Scenario 1) prioritized intra-district parity across 25.1% of grids, yielding moderate returns (0.93 cases/grid/year; efficiency ratio: 53.3). In contrast, Scenario 3 achieved the highest intervention efficiency: modifying vegetation in only 15.7% of grids (896 dual-vulnerable cells) captured over a quarter of total city-wide disease reduction, delivering 2.08 avoidable cases per intervened grid per year and an efficiency ratio of 118.8 (Table 3). This represents a 2.2-fold and 3.9-fold efficiency advantage over Scenarios 1 and 2, respectively, demonstrating that in land-constrained megacities, prioritizing greening in areas where high population density coincides with severe vegetation deficits offers the highest public health return on investment.

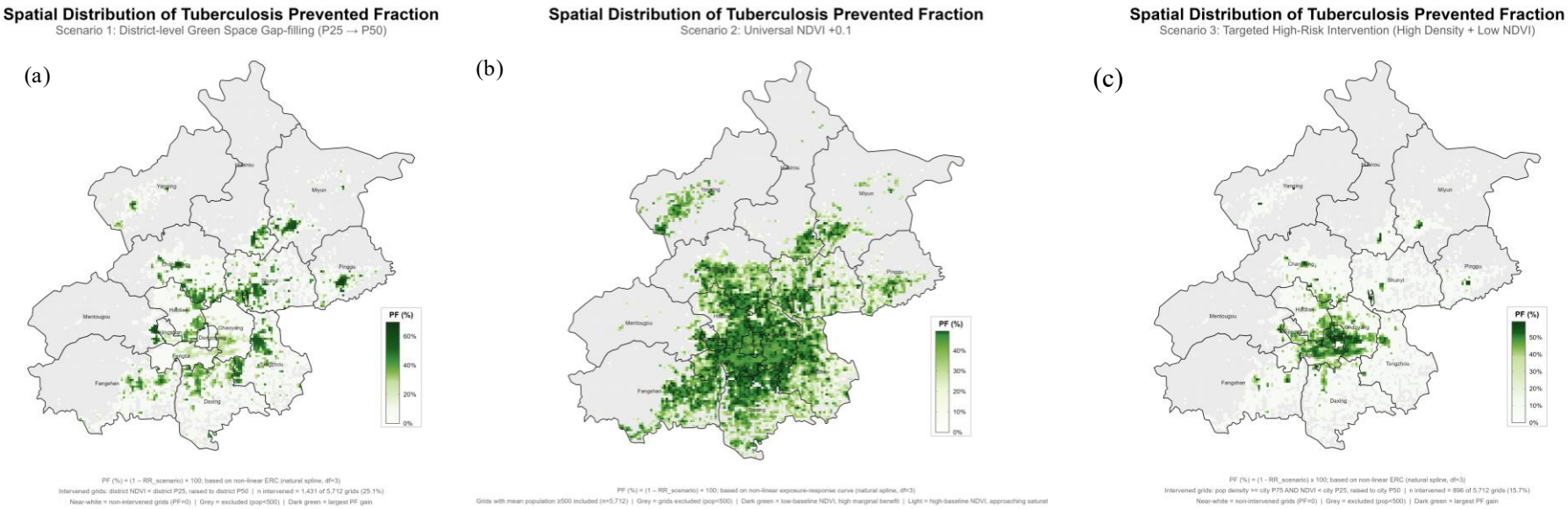


Figure 3. Spatial distribution of grid-level tuberculosis prevented fraction (PF, %) across three counterfactual greening scenarios in Beijing.

(a) Scenario 1: District-level green space gap-filling (raised grids with NDVI below the district-specific 25th percentile to the district-specific median).

(b) Scenario 2: Universal greening (+0.1 NDVI across all grids).

(c) Scenario 3: Targeted high-risk intervention (intervened only in grids simultaneously meeting population density above the city-wide 75th percentile and vegetation cover below the city-wide 25th percentile).

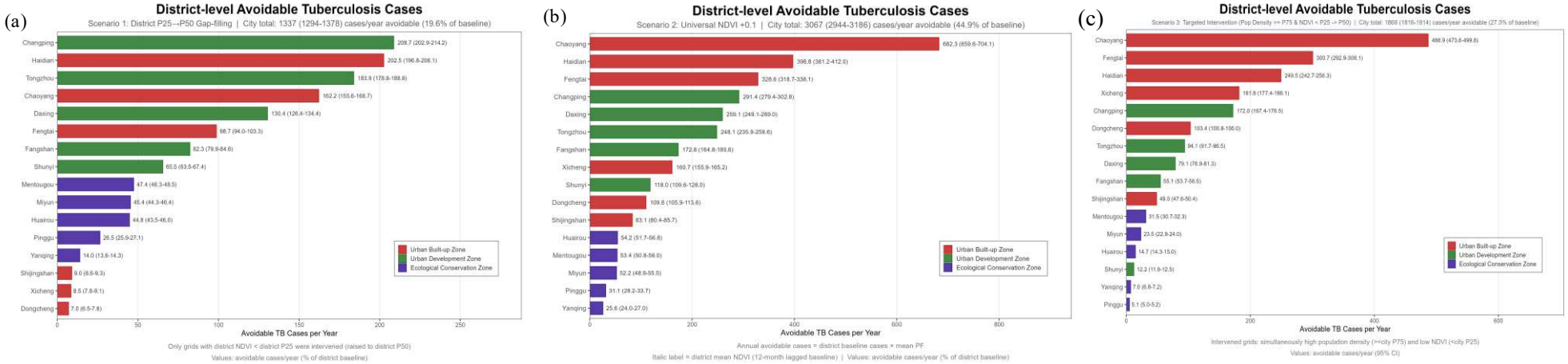


Figure 4. District-level annual avoidable tuberculosis cases under three policy scenarios across Beijing's planning zones.

Bars depict point estimates with 95% confidence intervals for **(a)** Scenario 1 (district-level gap-filling), **(b)** Scenario 2 (universal greening, +0.1 NDVI), and **(c)** Scenario 3 (targeted high-risk intervention). Districts are color-coded by their functional planning classifications: Urban Built-up Zone (red), Urban Development Zone (green), and Ecological Conservation Zone (purple), defined in accordance with the official spatial development guidelines of the Beijing Municipal People's Government. Numeric annotations denote the absolute annual avoidable case count and the percentage reduction relative to each district's historical baseline burden.

Table 3. Counterfactual Health Impact Assessment: Comparison of Three Green Space Improvement Scenarios for Tuberculosis Prevention in Beijing (2012–2024)

Parameter / Outcome	Scenario 1 District Gap-filling	Scenario 2 Universal (+0.1 NDVI)	Scenario 3 Targeted High-Risk
Panel A. Scenario Design Parameters			
Policy rationale	Equity-oriented: raise the lowest-greening grids within each district	Scale-oriented: uniform greening across all grids city-wide	Efficiency-oriented: prioritise dual-vulnerable grids (high density + low NDVI)
Eligibility criteria	Grid NDVI < district-specific P_{25}	All grids (no eligibility threshold)	Pop. density ≥ city-wide P_{75} AND NDVI < city-wide P_{25}
NDVI intervention target	District-specific median (P_{50}) (range: 0.258–0.419)	Baseline NDVI + 0.100 (fixed)	City-wide median (P_{50} = 0.374)
Mean NDVI increase in intervened grids (units)	0.072	0.100 (fixed)	0.092
n grids intervened / total (pop ≥500)	1,431 / 5,712	5,712 / 5,712	896 / 5,712
% grids intervened	25.1%	100.0%	15.7%
Panel B. City-wide Health Impact Estimates (Annual)			
City-wide baseline TB cases (cases/year)	6,827.5	6,827.5	6,827.5
Avoidable TB cases — point estimate (cases/year)	1,336.7	3,067.2	1,865.8
95% Confidence Interval	(1,294.6–1,377.9)	(2,944.3–3,185.2)	(1,816.2–1,913.9)
Prevented Fraction (PF%)	19.58%	44.92%	27.33%
95% Confidence Interval	(18.96%–20.18%)	(43.12%–46.65%)	(26.60%–28.03%)
Avoidable cases per intervened grid (cases/grid/year)	0.93	0.54	2.08
Efficiency ratio† (avoidable cases per 1% grids intervened)	53.3	30.7	118.8

ERC model: Natural cubic spline (*df*=3); Poisson two-way FE (district + year-month); offset=log(population); **Co-pollutants:** NO_2 and O_3 (lag 6m, VIF-selected); **Population filter:** grid mean population ≥500; **ERC reference point:** P_{10} (NDVI=0.279);

Note: Scenario eligibility thresholds were defined using multi-year (2012 – 2024) grid-level mean distributions (n = 5,712)

† Efficiency ratio = avoidable cases ÷ (% grids intervened). Higher values indicate greater health gain per unit of spatial resource allocated.

Significance: *** P<0.001. All three scenarios produced NDVI effect estimates significant at P<0.001.

4.Discussion

In this 13-year population-based study across Beijing, we systematically evaluated the spatiotemporal association between long-term residential greenness and active pulmonary tuberculosis incidence at a high-resolution 1-km grid scale. After rigorously adjusting for district-level spatial fixed effects, secular and seasonal temporal trends, time-varying meteorological factors, and collinearity-screened co-pollutants, long-term vegetation exposure ($NDVI_{MA12}$) exhibited a robust, independent protective association, with each one-IQR increase (0.102 units) corresponding to a 43.3% reduction in tuberculosis risk (IRR = 0.567).

While a growing body of epidemiological literature has recognized the broad health benefits of ambient green space(Ji et al., 2019; Twohig-Bennett and Jones, 2018), previous investigations into green space and tuberculosis have predominantly relied on coarse administrative aggregations or examined greenness as a modifying factor for air pollutant effects rather than as an independent exposure of primary interest(Yuan et al., 2025; Zhu et al., 2022). Studies using individual-level designs have confirmed that higher residential NDVI reduces TB mortality(Wang et al., 2022) and drug-resistant TB risk(Song et al., 2024), yet fine-grained incidence analyses incorporating non-linear dose-response modelling and prospective policy simulations remain scarce. Our findings advance current evidence in three key respects.

First, by tracking 5,712 populated 1-km grid cells over 13 consecutive years within a Poisson two-way fixed-effects framework, this study captures localized micro-environmental exposure contrasts that are systematically obscured in district-level analyses(Wang et al., 2025), while simultaneously circumventing over-controlling bias that would arise from grid-level fixed effects—which would absorb the very cross-sectional spatial variation in long-term greenery that constitutes our primary exposure of interest. Second, we identified a pronounced L-shaped, non-linear exposure-response trajectory-independently validated by non-parametric decile binning-demonstrating that protective benefits accrue most steeply across vegetation-deprived to moderate greenery levels (P_{10}-P_{50}), beyond which marginal returns diminish substantially. This saturation pattern mirrors non-linear dose-response relationships reported for green space and other chronic disease outcomes(Cao et al., 2025; Rojas-Rueda et al., 2019), and has direct implications for resource allocation. Third, translating these non-linear associations into

policy-oriented health impact assessments revealed that spatial targeting is paramount: an efficiency-driven strategy targeting dual-vulnerable grids (high density and low greenness, Scenario 3) achieved an intervention efficiency ratio nearly four times that of universal greening, averting over a quarter (27.33%) of the city-wide disease burden by modifying merely 15.7% of spatial grid cells .

At the baseline epidemiological level, our finding of a robust protective association between residential greenness and TB incidence is consistent with, yet reveals a substantially larger effect size than, earlier studies in China relying on coarse administrative aggregations(Yuan et al., 2025; Zhu et al., 2022). This discrepancy is largely methodological: district-level analyses inevitably induce exposure misclassification by smoothing out localized micro-environmental contrasts(Wang et al., 2025) , whereas our 1-km grid resolves greenness within immediate daily living spaces. Moreover, in a hyper-dense megacity such as Beijing — where baseline vegetation in built-up areas is severely constrained — incremental greenery is likely to operate in the steepest portion of the dose-response curve, yielding comparatively large marginal benefits, a pattern directly corroborated by the pronounced L-shaped ERC identified in this study.

The protective mechanism is biologically congruent with TB's chronic pathogenesis, whereby clinical disease predominantly arises from reactivation of latent *Mycobacterium tuberculosis* infection when cell-mediated immunity is compromised(Lönnroth et al., 2010) . Ambient vegetation is posited to reinforce host defense through multiple converging pathways: by alleviating chronic psychological stress and down-regulating cortisol-mediated immunosuppression(Jones et al., 2021; Twohig-Bennett and Jones, 2018) , by promoting outdoor activity and UV-B-driven vitamin D synthesis that upregulates cathelicidin expression in alveolar macrophages and directly enhances intracellular mycobacterial killing(Liu et al., 2006; Yamshchikov et al., 2010), and by filtering airborne pollutants that impair mucosal clearance(Barboza et al., 2021). Parameterized as a 12-month moving average ($NDVI_{MA12}$), our exposure metric directly captures this multi-month etiological window of cumulative host resistance while attenuating the intense seasonal vegetative oscillations characteristic of Beijing's temperate monsoon climate(Zhu et al., 2022).

A key contribution of this study is the characterization of a pronounced L-shaped,

non-linear exposure-response relationship between long-term residential greenness and tuberculosis incidence, a pattern that challenges the conventional log-linear assumption adopted in most prior environmental epidemiological analyses(Rojas-Rueda et al., 2019) . While non-linear NDVI-health associations have been reported for all-cause mortality and chronic disease(Martin et al., 2025), our study is among the first to demonstrate such a trajectory specifically for tuberculosis incidence using a continuous spline framework.

At the lower end of the greenness distribution (NDVI < P_{25} = 0.322), the exposure–response curve exhibited a markedly steep negative gradient, with relative risk declining from 1.327 at the 1st percentile to 0.544 at the median (NDVI = 0.374). This rapid risk reduction in vegetation-deprived zones is consistent with the principle that incremental greenery confers the greatest marginal health benefit where baseline exposure is most severely constrained(Qiu et al., 2026; Rojas-Rueda et al., 2019) , a pattern particularly salient in densely built urban environments where thermal stress, air stagnation, and absence of restorative outdoor spaces compound one another.

Conversely, as greenness exceeded approximately the 75th percentile (NDVI > 0.424), the protective gradient progressively attenuated toward an asymptotic lower bound (RR = 0.272 at P_{99}), consistent with diminishing marginal returns reported across green space-health dose-response analyses(Ge et al., 2021). We attribute this biological ceiling, in part, to the inherently indoor ecology of *M. tuberculosis* transmission: the bacterium spreads predominantly through sustained inhalation of infectious aerosols in poorly ventilated, overcrowded enclosed spaces —households, workplaces, and dormitories(Lee et al., 2022; Menon et al., 2026)— a proximal exposure pathway that ambient outdoor vegetation cannot fully attenuate regardless of its density. Once surrounding greenery reaches a threshold sufficient to optimize host immunocompetence and buffer pollution exposure, further vegetation gains yield negligible additional protection against transmission dynamics operating within built interiors.

Importantly, this non-linear trajectory was independently corroborated by our non-parametric decile binning analysis (Supplementary Figure S4). The categorical relative risks traced the continuous spline closely across all ten deciles without imposing parametric constraints on the functional form(Gasparrini et al., 2010), confirming that the steep initial mitigation and subsequent plateau reflect genuine epidemiological signal rather than modeling artifacts of spline knot placement.

Translating the exposure–response function into counterfactual scenarios reveals a fundamental trade-off between equity, scale, and spatial efficiency in urban greening. Universal greening (Scenario 2) maximized absolute burden reduction, yet much of its spatial footprint fell on peri-urban and ecological conservation zones already positioned on the saturated plateau of the exposure–response curve, yielding the lowest health return per intervened grid. District-level gap-filling (Scenario 1) promoted intra-district parity but delivered negligible relief to the historical core, where compressed internal vegetation variations offered minimal room for incremental improvement. By contrast, targeting dual-vulnerable grids (Scenario 3) achieved an efficiency ratio nearly four times that of universal greening while intervening in fewer than one-sixth of grids (Table 3).

These findings substantially extend emerging evidence that the spatial allocation of greening shapes its population health dividend as much as its total quantity. While previous health impact assessments have demonstrated substantial mortality reductions from universal green space access(Barboza et al., 2021) and expanded tree coverage(Iungman et al., 2023), a recent multi-city analysis across 96 C40 metropolises revealed that prioritizing greening in the most populous districts yielded approximately 2.7 times greater mortality benefits than uniform expansion(Martin et al., 2025) . Our findings demonstrate that this spatial efficiency dividend is not only preserved but markedly amplified in the context of an airborne chronic infectious disease. The larger efficiency multiplier observed here reflects two methodological and epidemiological features: first, our dual-vulnerability criterion concentrates interventions precisely where high host density (transmission pressure) coincides with severe vegetation deprivation (compromised resistance); second, the continuous non-linear spline explicitly penalizes greening investments in already-saturated ecological zones, preventing resource misallocation.

For land-constrained megacities, these results argue strongly against relying primarily on peripheral afforestation, which is administratively convenient but offers diminishing marginal health returns. Instead, compacted urban cores warrant fine-grained "urban acupuncture"—such as pocket parks, vegetated ventilation corridors, and rooftop or vertical greening capitalizing on vacated and fragmented plots (the municipal "vacate and regreen" initiative)(Mueller et al., 2020). Crucially, municipal authorities must remain attentive to the risk that environmental upgrading could induce green gentrification, inadvertently accelerating the displacement of

economically vulnerable residents who bear the highest baseline infection burden—the classic "just green enough" dilemma(Wolch et al., 2014) . Integrating high-resolution epidemiological vulnerability layers directly into statutory spatial master plans offers a robust pathway to ensure that public capital investments achieve the greatest, most equitable disease prevention.

This study has several notable strengths. Our high-resolution, 13-year grid-level panel design captures localized micro-environmental exposure gradients that are obscured in coarser administrative-unit analyses, while district-level and year-month fixed effects jointly account for unobserved spatial heterogeneity and temporal shocks. Co-pollutant confounding was addressed through variance inflation screening, and the resulting non-linear spline trajectory was independently corroborated by non-parametric decile binning. Translating these exposure–response functions into counterfactual policy scenarios further bridges abstract epidemiological risk estimates with actionable, efficiency-ranked spatial guidance.

Several limitations warrant consideration. First, as an ecological panel design, exposure was assigned at the residential 1-km grid level and cannot fully capture daily mobility, workplace exposure, or commuting patterns. Because such unmeasured activity-space variation is likely non-differential with respect to disease status, it would be expected to bias associations toward the null, suggesting that the true protective effect of greenness may be at least as large as, if not larger than, our estimates. Second, the surveillance registry lacked individual-level clinical and behavioral data — smoking history, indoor ventilation, comorbidities such as HIV or diabetes, and drug-resistance status. District fixed effects and time-varying covariates (population density, nighttime lights) absorb macro-level socioeconomic disparities, but residual confounding from unobserved individual risk factors cannot be entirely excluded. Third, NDVI captures horizontal, two-dimensional vegetative greenness but cannot distinguish vegetation structure (tree canopy versus shrub or grass), species composition, or public accessibility—attributes that differentially shape microclimatic cooling, pollutant filtration, and psychological restoration. Future work integrating LiDAR-derived canopy volume or street-view imagery could help disentangle which specific dimensions of urban greenery drive the protective association identified here.

5. Conclusion

This 13-year population-based panel study provides robust evidence that long-term residential greenness protects against active pulmonary tuberculosis in a hyper-dense megacity, following a pronounced L-shaped exposure–response relationship in which marginal protective gains are concentrated within vegetation-deprived built environments and diminish substantially thereafter. Crucially, our counterfactual evaluations demonstrate that the disease-mitigation dividend of urban green infrastructure depends fundamentally on spatial allocation rather than aggregate volume: prioritizing dual-vulnerable communities—where acute ecological deprivation coincides with high population crowding—yields disproportionately larger health returns than universal city-wide expansion. Whether this efficiency advantage generalizes to other megacities and airborne infectious diseases warrants further investigation. Nonetheless, embedding high-resolution epidemiological vulnerability metrics into municipal master planning offers an actionable, cost-effective blueprint to advance the WHO End TB Strategy and foster health-oriented, climate-resilient urban environments.

Declarations

Abbreviations

CDMet, China Daily Meteorological Dataset;
CHAP, ChinaHighAirPollutants;
CI, confidence interval;
CO, carbon monoxide;
COVID-19, coronavirus disease 2019;
df, degrees of freedom;
ERC, exposure–response curve;
FE, fixed effects;
HIV, human immunodeficiency virus;
HPA, hypothalamic–pituitary–adrenal;
IQR, interquartile range;
IRR, incidence rate ratio;
LiDAR, light detection and ranging;
LOESS, locally estimated scatterplot smoothing;
LTBI, latent tuberculosis infection.
MODIS, Moderate Resolution Imaging Spectroradiometer;
NDVI, normalized difference vegetation index;
NDVIMA6, 6-month backward moving average of NDVI;

NDVIMA12, 12-month backward moving average of NDVI;
NO_2, nitrogen dioxide;
NPP, Suomi National Polar-orbiting Partnership;
NTL, nighttime light intensity;
O_3, ozone;
PF, prevented fraction;
$PM_{2.5}$, particulate matter with an aerodynamic diameter of ≤2.5 μm;
PM_{10}, particulate matter with an aerodynamic diameter of ≤10 μm;
RR, relative risk;
SD, standard deviation;
SIN, sinusoidal projection;
SO_2, sulfur dioxide;
TB, tuberculosis;
UV-B, ultraviolet B radiation;
VIIRS, Visible Infrared Imaging Radiometer Suite;
VIF, variance inflation factor;
WHO, World Health Organization.

Ethics approval and consent to participate

This study did not involve any human intervention or clinical trials. Tuberculosis case data were obtained from routine public health surveillance activities in Beijing, China. The study was approved by **Beijing Center for Disease Control and Prevention Ethics Committee (approval number: BJCDC2026029).** Patient names were removed before the records were provided to the research team. Residential addresses were used for geocoding, and the analyses were conducted using monthly case counts aggregated to 1-km × 1-km grid cells.This study was conducted in accordance with the principles of the Declaration of Helsinki.

Consent for publication

Not applicable.

Availability of data and materials

The individual-level tuberculosis notification data used in this study were provided by the Beijing Center for Disease Control and Prevention. These data are not publicly available because the data provider does not permit their public release. The

environmental and population data sources are described in Section 2.2 and the corresponding references.

Competing interests

The authors declare that they have no competing interests.

Funding

This project was financially supported by the Capital's Funds for Health Improvement and Research (2026-2G-30114).

Authors' contributions

Ze Zeng performed the data analysis and drafted the manuscript. Wenyi Zhang contributed to study conceptualization and data validation. Zanmei Wei performed the matching of environmental data to the study grids. Zhidong Gao contributed to discussions of the study. Yuxiao Wang contributed to the data analysis. Junyu He contributed to study conceptualization. Hengliang Lv and Yuming Guo contributed to manuscript checking. Xingshu Chen reviewed the initial manuscript draft. Jie Li provided the tuberculosis data and contributed to discussions of the study. Shanhua Sun contributed to manuscript writing and final manuscript checking.
Ze Zeng, Wenyi Zhang, and Zanmei Wei contributed equally to this work and share first authorship. Xingshu Chen, Jie Li , and Shanhua Sun are corresponding authors.

Acknowledgements

We thank the Beijing Center for Disease Control and Prevention for providing the tuberculosis notification data used in this study.

References

Barboza, E.P., Cirach, M., Khomenko, S., Iungman, T., Mueller, N., Barrera-Gómez, J., Rojas-Rueda, D., Kondo, M., Nieuwenhuijsen, M., 2021. Green space and mortality in European cities: a health impact assessment study. The Lancet Planetary Health 5, e718–e730. https://doi.org/10.1016/S2542-5196(21)00229-1

Cao, W., Wang, L., Wang, J., Elsadek, M., Zhang, D., 2025. Nonlinear health benefits of public green space: evidence from a nationwide machine learning study in China. Front. Public

Health 13, 1680591. https://doi.org/10.3389/fpubh.2025.1680591

Chen, Z., Yu, B., Yang, C., Zhou, Y., Yao, S., Qian, X., Wang, C., Wu, B., Wu, J., 2021. An extended time series (2000–2018) of global NPP-VIIRS-like nighttime light data from a cross-sensor calibration. Earth Syst. Sci. Data 13, 889–906. https://doi.org/10.5194/essd-13-889-2021

Didan, K., 2021. MODIS/Terra Vegetation Indices Monthly L3 Global 1km SIN Grid V061. https://doi.org/10.5067/MODIS/MOD13A3.061

Furin, J., Cox, H., Pai, M., 2019. Tuberculosis. The Lancet 393, 1642–1656. https://doi.org/10.1016/S0140-6736(19)30308-3

Gasparrini, A., Armstrong, B., Kenward, M.G., 2010. Distributed lag non-linear models. Statistics in Medicine 29, 2224–2234. https://doi.org/10.1002/sim.3940

Ge, E., Gao, J., Ren, Z., Liu, X., Luo, M., Zhong, J., Fei, F., Chen, B., Wang, X., Wei, X., Peng, Y., 2021. Greenness exposure and all-cause mortality during multi-drug resistant tuberculosis treatment: A population-based cohort study. Science of The Total Environment 771, 145422. https://doi.org/10.1016/j.scitotenv.2021.145422

Hui, D., Sahu, S., Ditiu, L., Marais, B.J., Yeboah-Manu, D., Goletti, D., Walzl, G., Zumla, A., 2026. Global tuberculosis response off track: urgent priorities to end the world's top infectious killer. The Lancet 407, 1126–1129. https://doi.org/10.1016/S0140-6736(25)02433-X

Iungman, T., Cirach, M., Marando, F., Pereira Barboza, E., Khomenko, S., Masselot, P., Quijal-Zamorano, M., Mueller, N., Gasparrini, A., Urquiza, J., Heris, M., Thondoo, M., Nieuwenhuijsen, M., 2023. Cooling cities through urban green infrastructure: a health impact assessment of European cities. The Lancet 401, 577–589. https://doi.org/10.1016/S0140-6736(22)02585-5

Ji, J.S., Zhu, A., Bai, C., Wu, C.-D., Yan, L., Tang, S., Zeng, Y., James, P., 2019. Residential greenness and mortality in oldest-old women and men in China: a longitudinal cohort study. The Lancet Planetary Health 3, e17–e25. https://doi.org/10.1016/S2542-5196(18)30264-X

Jones, R., Tarter, R., Ross, A.M., 2021. Greenspace Interventions, Stress and Cortisol: A Scoping Review. IJERPH 18, 2802. https://doi.org/10.3390/ijerph18062802

Lee, J.-Y., Kwon, N., Goo, G., Cho, S., 2022. Inadequate housing and pulmonary tuberculosis: a systematic review. BMC Public Health 22, 622. https://doi.org/10.1186/s12889-022-12879-6

Liu, P.T., Stenger, S., Li, H., Wenzel, L., Tan, B.H., Krutzik, S.R., Ochoa, M.T., Schauber, J., Wu, K., Meinken, C., Kamen, D.L., Wagner, M., Bals, R., Steinmeyer, A., Zügel, U., Gallo, R.L., Eisenberg, D., Hewison, M., Hollis, B.W., Adams, J.S., Bloom, B.R., Modlin, R.L., 2006. Toll-Like Receptor Triggering of a Vitamin D-Mediated Human Antimicrobial Response. Science 311, 1770–1773. https://doi.org/10.1126/science.1123933

Lönnroth, K., Castro, K.G., Chakaya, J.M., Chauhan, L.S., Floyd, K., Glaziou, P., Raviglione, M.C., 2010. Tuberculosis control and elimination 2010–50: cure, care, and social development. The Lancet 375, 1814–1829. https://doi.org/10.1016/S0140-6736(10)60483-7

Martin, G.K., Rojas-Rueda, D., Fong, K.C., Jimenez, M.P., Kinney, P.L., Canales, R., Anenberg, S.C., 2025. A health impact assessment of progress towards urban nature targets in the 96 C40 cities. The Lancet Planetary Health 9, e284–e293. https://doi.org/10.1016/S2542-5196(25)00053-1

Menon, S., Harries, A., Dlodlo, R., Badoum, G., Dogo, M., Mbitikon, O., Sinha, P., Lin, Y., Jaju, J.,

Soe, A., Singh, A., Kalottee, B., Koura, K., 2026. Series 1: Behind the Spread: A Scoping Review of Risk Factors for Exposure to Mycobacterium tuberculosis. TropicalMed 11, 58. https://doi.org/10.3390/tropicalmed11020058

Mueller, N., Rojas-Rueda, D., Khreis, H., Cirach, M., Andrés, D., Ballester, J., Bartoll, X., Daher, C., Deluca, A., Echave, C., Milà, C., Márquez, S., Palou, J., Pérez, K., Tonne, C., Stevenson, M., Rueda, S., Nieuwenhuijsen, M., 2020. Changing the urban design of cities for health: The superblock model. Environment International 134, 105132. https://doi.org/10.1016/j.envint.2019.105132

Prasad, A., Ross, A., Rosenberg, P., Dye, C., 2016. A world of cities and the end of TB. Trans R Soc Trop Med Hyg 110, 151–152. https://doi.org/10.1093/trstmh/trw004

Qiu, M., Browning, M.H.E.M., Zhang, R., Hong, Y., Chen, S., Li, H., Xia, T., Mao, Y., Xian, Z., Zhang, J., 2026. Dose thresholds of urban nature contact for human health: A critical scoping review. Environmental Impact Assessment Review 121, 108495. https://doi.org/10.1016/j.eiar.2026.108495

Rojas-Rueda, D., Nieuwenhuijsen, M.J., Gascon, M., Perez-Leon, D., Mudu, P., 2019. Green spaces and mortality: a systematic review and meta-analysis of cohort studies. The Lancet Planetary Health 3, e469–e477. https://doi.org/10.1016/S2542-5196(19)30215-3

Sims, K., Reith, A., Bright, E., Kaufman, J., Pyle, J., Epting, J., Gonzales, J., Adams, D., Powell, E., Urban, M., Rose, A., n.d. LandScan Global 2022. https://doi.org/10.48690/1529167

Song, W., Liu, Yi, Men, D., Li, S., Tao, N., Zhang, Q., Liu, S., An, Q., Zhu, X., Han, Q., Zhang, Y., Li, Ying-ying, Li, C., Liu, Yao, Yu, C., Li, Yi-fan, Li, H., 2024. Associations of residential greenness exposure and ambient air pollutants with newly-diagnosed drug-resistant tuberculosis cases. Environ Sci Pollut Res 31, 27240–27258. https://doi.org/10.1007/s11356-024-32913-x

Twohig-Bennett, C., Jones, A., 2018. The health benefits of the great outdoors: A systematic review and meta-analysis of greenspace exposure and health outcomes. Environmental Research 166, 628–637. https://doi.org/10.1016/j.envres.2018.06.030

Wang, X.-Q., Zhang, K.-D., Yu, W.-J., Zhao, J.-W., Huang, K., Hu, C.-Y., Zhang, X.-J., Kan, X.-H., 2022. Associations of exposures to air pollution and greenness with mortality in a newly treated tuberculosis cohort. Environ Sci Pollut Res 30, 34229–34242. https://doi.org/10.1007/s11356-022-24433-3

Wang, Yaping, Liu, X., Li, Y., Liu, M., Wang, Yiheng, Zhang, H., Liu, J., Zhao, Y., 2025. Association of urbanization-related factors with tuberculosis incidence among 1992 counties in China from 2005 to 2019: a nationwide observational study. Infect Dis Poverty 14, 30. https://doi.org/10.1186/s40249-025-01299-4

Wei, J., Li, Z., Cribb, M., Huang, W., Xue, W., Sun, L., Guo, J., Peng, Y., Li, J., Lyapustin, A., Liu, L., Wu, H., Song, Y., 2020. Improved 1 km resolution $PM_{2.5}$ estimates across China using enhanced space–time extremely randomized trees. Atmos. Chem. Phys. 20, 3273–3289. https://doi.org/10.5194/acp-20-3273-2020

Wei, J., Li, Z., Wang, J., Li, C., Gupta, P., Cribb, M., 2023. Ground-level gaseous pollutants (NO_2 , SO_2 , and CO) in China: daily seamless mapping and spatiotemporal variations. Atmos. Chem. Phys. 23, 1511–1532. https://doi.org/10.5194/acp-23-1511-2023

Wolch, J.R., Byrne, J., Newell, J.P., 2014. Urban green space, public health, and environmental

justice: The challenge of making cities 'just green enough.' Landscape and Urban Planning 125, 234–244. https://doi.org/10.1016/j.landurbplan.2014.01.017

Yamshchikov, A.V., Kurbatova, E.V., Kumari, M., Blumberg, H.M., Ziegler, T.R., Ray, S.M., Tangpricha, V., 2010. Vitamin D status and antimicrobial peptide cathelicidin (LL-37) concentrations in patients with active pulmonary tuberculosis. The American Journal of Clinical Nutrition 92, 603–611. https://doi.org/10.3945/ajcn.2010.29411

Yang, Z., Li, Z., Cheng, F., Lv, Q., Li, K., Zhang, T., Zhou, Y., Zhao, B., Xue, W., Wei, J., 2025. Two-decade surface ozone (O3) pollution in China: Enhanced fine-scale estimations and environmental health implications. Remote Sensing of Environment 317, 114459. https://doi.org/10.1016/j.rse.2024.114459

Yuan, D., Xie, B., Pang, Z., Liu, K., Chen, B., 2025. Short- and long-term exposure to ambient air pollution and greenness in relation to pulmonary tuberculosis incidence. Sci Rep 15, 25594. https://doi.org/10.1038/s41598-025-11465-1

Zenner, D., Hui, D.S., Sahu, S., Ditiu, L., Yeboah-Manu, D., Ntoumi, F., Mfinanga, S., Chakaya, J., Zumla, Adam, Ahmed, R., Tiberi, S., Goletti, D., Walzl, G., Marais, B.J., Zumla, Alimuddin, 2026. State of the global tuberculosis epidemic: burden, progress towards WHO End TB Strategy targets and systemic challenges. The Lancet Microbe 101433. https://doi.org/10.1016/j.lanmic.2026.101433

Zhang, J., Liu, B., Ren, S., Han, W., Ding, Y., Peng, S., 2024. A 4 km daily gridded meteorological dataset for China from 2000 to 2020. Sci Data 11, 1230. https://doi.org/10.1038/s41597-024-04029-x

Zhu, S., Wu, Y., Wang, Q., Gao, L., Chen, L., Zeng, F., Yang, P., Gao, Y., Yang, J., 2022. Long-term exposure to ambient air pollution and greenness in relation to pulmonary tuberculosis in China: A nationwide modelling study. Environmental Research 214, 114100. https://doi.org/10.1016/j.envres.2022.114100

Supplementary Files

This is a list of supplementary files associated with this preprint. Click to download.

- FigS4.png
- FigS2.png
- FigS1.png
- FigS3.png